Next Energy 8 (2025) 100248

Contents lists available at ScienceDirect

Next Energy

journal homepage: www.sciencedirect.com/journal/next-energy

Research article

# Enhanced p-doping and efficiency in organic solar cells using Mg and Pd ions at the HTL/PTB7 interface

Jin Hee Lee[a], Merve Nur Ekmekci[b], Yeasin Khan[a,c], Bright Walker[c,*], Jung Hwa Seo[a,*]

[a] Department of Physics, University of Seoul, Seoul, 02504, Republic of Korea
[b] Institute of Nanotechnology, Karlsruhe Institute of Technology, Karlsruhe, 76131, Germany
[c] Department of Chemistry, Kyung Hee University, Seoul, 02447, Republic of Korea

ARTICLE INFO

*Keywords:*
Interface analysis
X-ray and ultraviolet photoelectron spectroscopy
Organic solar cell

ABSTRACT

This study investigates the application of new hole transport layers (HTLs) integrating magnesium and palladium metals with the organic polymer poly(styrene sulfonate) (PSS) in organic solar cells (OSCs). When used alone, these HTLs exhibited various drawbacks; however, blending them with the benchmark material PEDOT:PSS mitigated these issues and improved efficiency. Ultraviolet photoelectron spectroscopy (UPS) and X-ray photoelectron spectroscopy (XPS) measurements provided a detailed understanding of the interfacial energy level alignment, electronic band structure, and band bending at the HTL/PTB7 interface. Single Mg:PSS and Pd:PSS OSCs showed efficiencies of 6.232 and 5.836%, respectively. The relatively low open-circuit voltage ($V_{OC}$) and fill factor (FF) were attributed to Auger recombination under light intensity. UPS and XPS also indicated that the hole extraction capability of PTB7 was hindered, leading to recombination at the barrier. By blending with PEDOT:PSS, the efficiencies of Mg:PSS and Pd:PSS were improved to 8.356 and 8.303%, respectively. This improvement was due to reduced current leakage, resulting from higher shunt resistance and lower series resistance, as observed in dark current measurements. Additionally, the formation of ohmic contacts at the HTL/PTB7 interface enhanced hole extraction and reduced recombination. This study underscores the potential of mixed organic-metal HTL structures in OSCs to modulate energy band structures, providing insights into the selection of metal-organic combinations for optimizing OSC efficiency and performance.

## 1. Introduction

Organic solar cells (OSCs) are one of the most promising next-generation photovoltaic technologies capable of generating electricity from solar energy. OSCs have high industrial value due to their light weight, low energy fabrication process, and excellent potential for large-area printing, making continued research into economical approaches to achieving high power conversion efficiency (PCE) a significant area of interest [1–4]. The enhancement of PCE can be achieved through various methods. Single bulk heterojunction (BHJ) polymer solar cells have reached up to 18% efficiency with the development of new donor and acceptor materials [5,6]. Continuous efforts are being made to develop new donors and acceptors, with non-fullerene acceptors significantly contributing to groundbreaking efficiency improvements [7–9]. In addition to the active layer, the interface between the active layer and the electrodes plays a crucial role in the charge transport mechanisms of holes and electrons. The hole transport layer (HTL) and the electron transport layer (ETL) prioritize the transport and extraction capabilities of each carrier from the active layer [10–13]. Moreover, these layers help capture carriers moving in the opposite direction, reducing leakage current and ensuring proper current flow. Several types of materials demonstrating these properties have been explored for use as HTLs in BHJ solar cells, including conductive polymers [14,15], metal oxides [16–20], conjugated polyelectrolytes (CPEs) [21–23], cross-linkable materials [24,25], and graphene-based materials [26].

A well-defined interlayer is essential for achieving high efficiency and stability in solar cells. Among organic materials, poly (3,4-ethylenedioxythiophene): poly (styrene sulfonate) (PEDOT:PSS) is the dominant material for efficient hole extraction [27–29]. PEDOT:PSS with its high work function (around 5.1 eV) and excellent conductivity, is often used to achieve high PCE. PEDOT:PSS has undergone various technological advancements, including novel chemical modifications, metal-ion doping techniques, and scalability for large-area printing, making it

* Corresponding authors.
*E-mail addresses:* walker@khu.ac.kr (B. Walker), seojh@uos.ac.kr (J.H. Seo).

https://doi.org/10.1016/j.nxener.2025.100248
Received 22 November 2024; Received in revised form 30 December 2024; Accepted 28 January 2025

an essential component in the technological development of next-generation optoelectronic devices [30–32]. However, PEDOT:PSS has a high acidic content, which can negatively impact the long-term operational stability of OSCs [11,33]. Studies have shown that the strong acidity of PEDOT:PSS can degrade the underlying electrode, allowing dissociated metal elements to infiltrate the active layer, severely affecting the efficiency of OSCs. In previous studies, we fabricated metal:PSS and analyzed the electronic structure to understand the mechanism of the interfacial layer, and reported the performance of perovskite solar cells [34,35]. Among these, we selected 2 divalent cations with distinct electronic structure characteristics for further experiments.

In our present work, we replaced the PEDOT:PSS component with ions of different sizes, specifically Mg and Pd, to create Mg:PSS and Pd:PSS, which were then incorporated into PTB7:$PC_{71}BM$ solar cells. The choice of Mg and Pd ions was based on their differing ionic sizes and potential to modify the interfacial properties and energy levels of the HTL. Mg ions, with their smaller ionic radius, are expected to improve film formation and stability, while Pd ions, with their larger ionic radius, can enhance conductivity and work function alignment with the active layer. To retain the benefits of PEDOT:PSS, such as high work function and excellent conductivity, a small amount of PEDOT:PSS was mixed with Mg and Pd to produce a stable and efficient HTL. The interlayer characteristics of Mg and Pd and the energy level alignment between the interlayer and donor were investigated using ultraviolet photoelectron spectroscopy (UPS) and X-ray photoelectron spectroscopy (XPS), allowing us to construct an energy level diagram. This study compares OSCs with metal-doped HTLs as a potential replacement for PEDOT:PSS.

## 2. Materials and method

### 2.1. Materials

The preparation method of Mg:PSS is as follows: 5 mL of a $MgCl_2$ (1.45 mg/8 mL methanol) solution was added to 3 mL of a commercial H:PSS solution to form a clear solution. This solution was diluted with 15 mL of isopropyl alcohol (IPA), resulting in the precipitation of the polymer. The precipitated polymer was centrifuged and re-dissolved in 1.5 mL of an aqueous $MgCl_2$ solution, then diluted with 20 mL of methanol to precipitate the polymer again. The same process was repeated with the remaining $MgCl_2$ solution. The repeated interactions with the $MgCl_2$ solution facilitated the removal of HCl and the incorporation of Mg ions, promoting the formation of Mg:PSS. After the third precipitation, the polymer was re-dissolved in 5 mL of $H_2O$, re-precipitated twice in IPA, and washed with IPA and hexane. Finally, the polymer was dried in a glove box (under $N_2$ atmosphere) to obtain Mg:PSS.

The Pd:PSS preparation process is as follows: 0.219 g of palladium acetate was dissolved in 24 mL of methanol and added to 1 mL of the H:PSS solution. The mixture was sonicated for 20 seconds, precipitated in IPA, and centrifuged. The dark brown precipitate was separated, dissolved in distilled water, and re-precipitated in IPA. The precipitate was washed several times with IPA and dried in a glove box to obtain Pd:PSS.

### 2.2. Device fabrication

The structure of the organic solar cells, Glass/ITO/HTL/PTB7:$PC_{71}BM$/PFN-Br/Al, was fabricated on glass substrates coated with indium tin oxide (ITO). The substrates were first cleaned using a detergent solution, followed by sequential sonication in deionized water, acetone, and isopropyl alcohol for 20 min each. The HTLs used were Mg:PSS, Pd:PSS, and 2 other types: Mg:PSS and Pd:PSS doped with 5% (50 μL) PEDOT:PSS. Each of the 4 types of HTL was filtered using a 0.45 μm cellulose acetate syringe filter and spin-coated onto the substrates, followed by annealing at 100 °C for 10 min. After the films cooled to room temperature, the substrates were transferred into a nitrogen-filled glove box where the polymer blend of PTB7:$PC_{71}BM$ (1:1.5 in CB 3%v/v DIO) was spin-coated onto the HTL-coated substrates at 1300 rpm for 60 seconds, followed by annealing at 80 °C for 10 min to form the active layer. For the ETL, PFN-Br was dissolved in methanol and spin-coated onto the active layer at 2000 rpm for 60 seconds. Finally, aluminum (100 nm) was deposited via thermal evaporation through a shadow mask under a pressure of approximately $3 \times 10^6$ bar to complete the device, resulting in an active area of 0.124 $cm^2$.

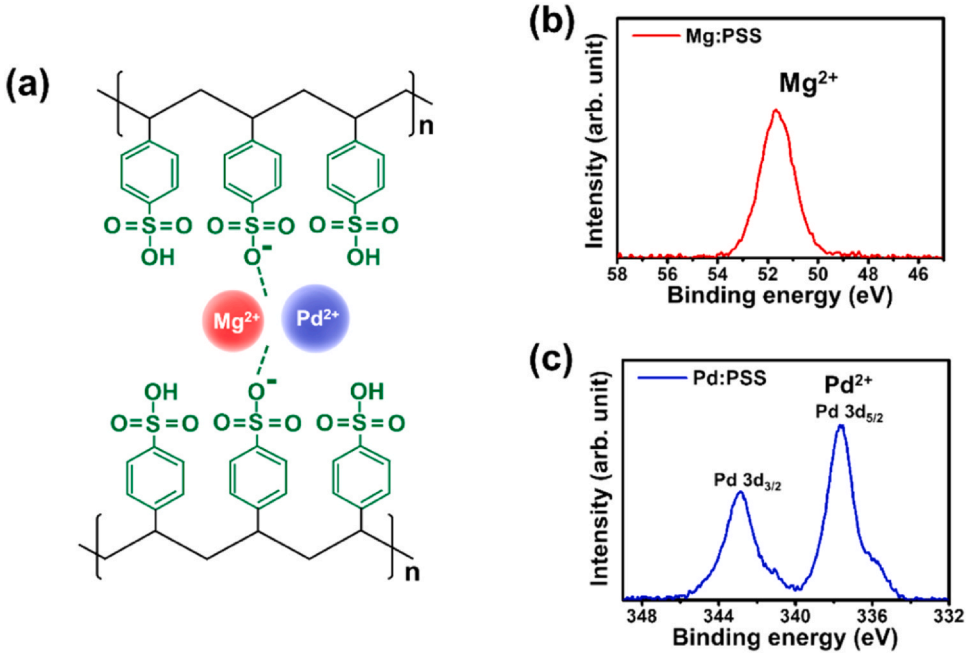


**Fig. 1.** (a) Materials structures of Mg:PSS and Pd:PSS, (b) Ion states of Mg:PSS and Pd:PSS analyzed via XPS. PSS = poly (styrene sulfonate); XPS = X-ray photoelectron spectroscopy.

### 2.3. Device characterization

The current-voltage (J-V) characteristics of the solar cell devices were measured using a Keithley 2635 source-measure unit under A.M 1.5 G illumination with an intensity of 100 mW/cm$^2$. The intensity of the simulated sunlight from a Xe arc lamp was calibrated immediately before testing using a certified reference silicon photodiode. The external quantum efficiency (EQE) measurements were performed using a QEX7 system from PV Measurements, Inc. The UPS and XPS spectra were obtained using a Thermo Fisher Scientific ESCALAB 250XI.

## 3. Results and discussion

Fig. 1 shows the structures and ion states of Mg:PSS and Pd:PSS. To develop an effective p-type polymer electrolysis material, we fabricated metal:PSS and electronic structures, and perovskite solar cells through preliminary research [34,35]. Metal:PSS compensates for the high concentration of p-type carriers in the semiconductor by allowing metal ions to easily accept electrons from the active layer semiconductor. We selected Mg and Pd, both bound with the same divalent cation, for comparative analysis (Fig. 1a). Fig. 1(b) and (c) show that the ion states of bonded Mg and Pd were properly formed. In the case of Pd:PSS, Pd$^0$ was observed at 336 eV, indicating that even with the same divalent cation, it exhibits different bonding characteristics compare to PSS, an organic material.

To demonstrate the application of Pd:PSS and Mg:PSS as HTL, device optimization was performed with the PTB7:PC$_{71}$BM solar cell structure. The current density-voltage characteristic curves of the Mg:PSS and Pd:PSS BHJ solar cells under AM 1.5 G illumination are shown in Fig. 2(a). A comparison of photovoltaic parameters to characteristic curves is summarized in Table 1. A J-V characteristic curve of a control OSCs using regular PEDOT:PSS is included in the Supporting Information (Fig. S1). The thicknesses were fine-tuned for device optimization. The efficiency of both devices was optimized at 0.3 mg/1 mL, and the amount of PEDOT:PSS was adjusted to improve overall performance by mixing PEDOT:PSS in an amount of 5%. The efficiency of the optimized single devices was 6.232% (Mg) and 5.836% (Pd), respectively, showing improvement over 5.749% (without HTL), but fill factor (FF) and open-circuit voltage ($V_{OC}$) recorded low values. Although both are divalent cations, it was expected that they would show different properties and efficiencies due to the different sizes of the ions themselves. However, Mg:PSS and Pd:PSS were almost similar. Blending with PEDOT:PSS increased the efficiency-determining parameters $V_{OC}$ and FF, resulting in PCEs of 8.356% (Mg:PEDOT:PSS) and 8.303% (Pd:PEDOT:PSS). A total of 6 optimized OSC devices, including the one without an HTL, were periodically measured in air to evaluate their stability, as shown in Fig. S2. All devices with metal ions exhibited improved average stability compared to the single-layer PEDOT:PSS device. Notably, after 168 h, the stability of Mg:PEDOT:PSS decreased to 47.6%, while PEDOT:PSS dropped to 16.5% (based on 100% at the initial measurement at 0 h). Furthermore, after 194 h, the efficiency of all devices with metal ions remained above 30%, demonstrating an overall improvement in stability.

The EQE of devices using 4 different HTLs (Pd:PSS, Mg:PSS, Pd:PEDOT:PSS, Mg:PEDOT:PSS) was observed across the entire absorption spectrum (400–1000 nm) (Fig. 2b). The integrated current densities for the 4 HTLs (Pd:PSS, Mg:PSS, Pd:PEDOT:PSS, Mg:PEDOT:PSS) are 17.708, 16.975, 18.214, and 16.964 mA/cm$^2$, respectively. Compared to the device without an HTL, devices using the 4 HTLs showed enhanced photocurrent generation across all regions, which can be attributed to the optical interference effect. The use of these 4 HTLs increases the charge carrier generation rate, leading to a

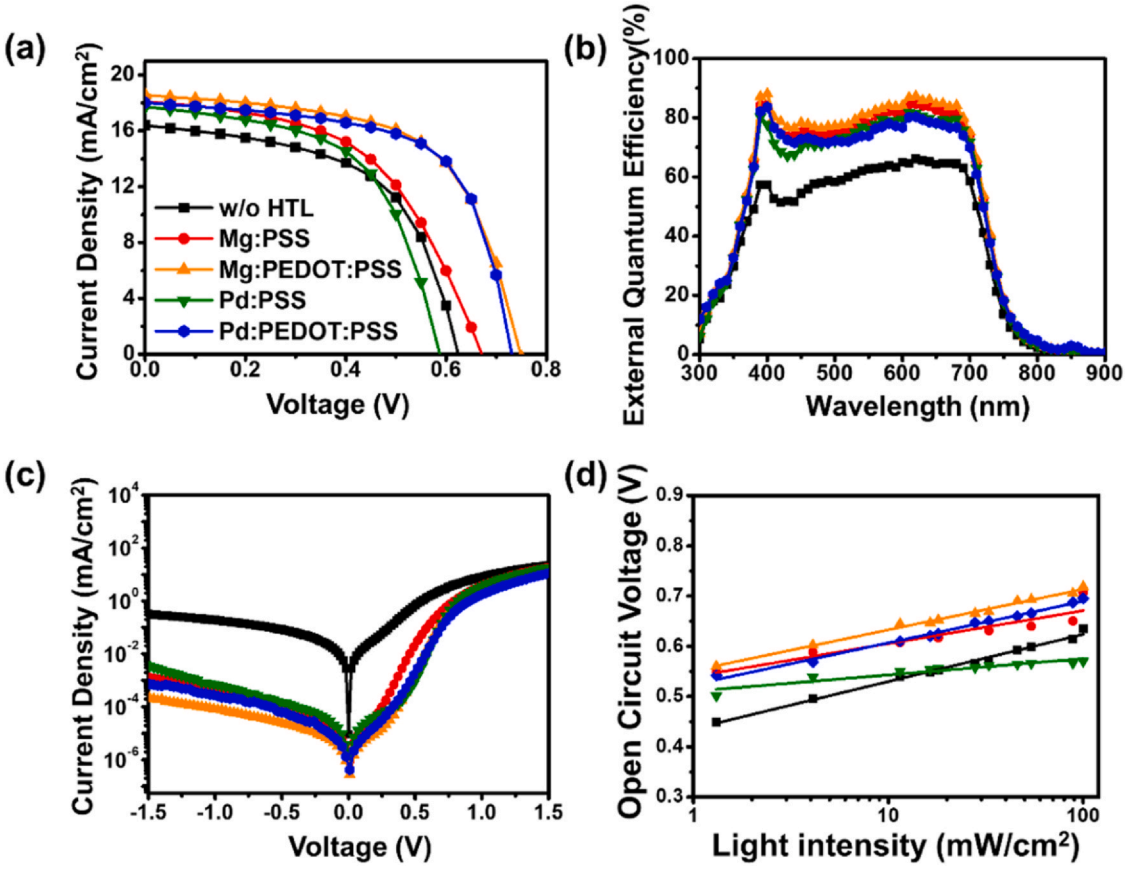


**Fig. 2.** (a) J-V characteristics, (b) External quantum efficiency spectra, (c) Dark J-V characteristics, and (d) Light dependence of organic solar cell with Mg:PSS, Pd:PSS and PEDOT:PSS-blended Mg:PSS, Pd:PSS. PEDOT:PSS = poly (3,4-ethylenedioxythiophene): poly (styrene sulfonate).

**Table 1**
Photovoltaic parameters of the OSC with Mg:PSS, Pd:PSS, Mg:PEDOT:PSS, Pd:PEDOT:PSS

| HTLs | $J_{SC}$ (mA·cm$^{-2}$) | $J_{SC\text{-}EQE}$ (mA·cm$^{-2}$) | $V_{OC}$ (V) | FF (%) | PCE (%) | |
|---|---|---|---|---|---|---|
| | | | | | Best | Average |
| w/o | 16.146 ± 0.282 | 13.669 | 0.565 ± 0.057 | 50.288 ± 0.061 | 5.749 | 4.639 ± 1.003 |
| Mg:PSS | 17.529 ± 0.571 | 17.708 | 0.667 ± 0.038 | 48.707 ± 0.024 | 6.232 | 5.691 ± 0.449 |
| Mg:PEDOT:PSS | 18.167 ± 0.223 | 18.214 | 0.736 ± 0.009 | 62.157 ± 0.018 | 8.356 | 8.311 ± 0.167 |
| Pd:PSS | 17.227 ± 0.763 | 16.975 | 0.593 ± 0.020 | 51.549 ± 0.029 | 5.836 | 5.260 ± 0.345 |
| Pd:PEDOT:PSS | 18.071 ± 0.043 | 16.964 | 0.733 ± 0.009 | 60.725 ± 0.026 | 8.303 | 8.042 ± 0.263 |

EQE = external quantum efficiency; FF = fill factor; HTLs = hole transport layers; OSC = organic solar cell; PCE = power conversion efficiency; PEDOT:PSS = poly (3,4-ethylenedioxythiophene): poly (styrene sulfonate); $V_{OC}$ = open-circuit voltage; $J_{SC}$ = short-circuit current density.

**Table 2**
Dark J-V characteristic and Light dependence of the OSC

| HTLs | $R_{Sh}$ (Ohm·m$^2$) | $R_S$ (Ohm·cm$^2$) | Ideality factor (kT/q) |
|---|---|---|---|
| w/o | 83.718 | 34.964 | 1.58 |
| Mg:PSS | 816.810 | 19.043 | 1.01 |
| Mg:PEDOT:PSS | 2585.600 | 19.051 | 1.36 |
| Pd:PSS | 505.960 | 21.286 | 0.54 |
| Pd:PEDOT:PSS | 2043.000 | 21.152 | 1.39 |

HTLs = hole transport layers; OSC = organic solar cell; PEDOT:PSS = poly (3,4-ethylenedioxythiophene): poly (styrene sulfonate); $R_{Sh}$ = shunt resistance; $R_S$ = series resistance.

higher device short-circuit current density ($J_{SC}$), and this phenomenon is maintained even when PEDOT:PSS is blended.

To understand the impact of the types of metals, Pd and Mg, on OSC characteristics, we characterized the series resistance and shunt resistance from dark J-V characteristic (Fig. 2c). Analyzing shunt and series resistance helps to understand the effect of HTLs on OSCs. Detailed parameters are shown in Table 2. High shunt resistance and low series resistance provide better device performance under illumination by reducing $J_{SC}$ and FF losses. The shunt resistances for single Mg:PSS and Pd:PSS are 816.810 Ω·cm$^2$ and 505.960 Ω·cm$^2$, respectively, which are significantly higher than the shunt resistance of the device without HTL (83.718 Ω·cm$^2$). This indicates that the absence of an HTL results in photocarrier loss. While the series resistance remained similar even when blending with PEDOT:PSS, the shunt resistance increased by 3.16 (Mg:PSS), 4.04 (Pd:PSS) times compared to the devices without PEDOT:PSS. High shunt resistance and low series resistance in the device enhance performance by reducing current leakage and photocarrier loss.

By measuring the light intensity dependence of $V_{OC}$, we can determine the type of recombination on which they depend. Fig. 2(d) depicts $V_{OC}$ as a function of illumination intensity and fits the following equation: [36,37]

$$V_{OC} = \left(\frac{KT}{q}\right) In\left(\frac{J_{SC}}{J_0} + 1\right)$$

where $k$ is the Boltzmann constant, $q$ is the electronic charge, $T$ is the temperature in Kelvin, and $J_0$ is the saturation current density (dark). The anomaly coefficient ($n$), which describes the slope of the data relative to kT/q, provides information about which type of recombination dominates the losses in the device [38–41]. When the slope of the ideality factor is close to 1, bimolecular recombination is dominant, whereas a slope close to 2 indicates monomolecular recombination. Monomolecular recombination involves a high number of recombinations due to trap states, leading to many traps. Bimolecular recombination relies on band-to-band recombination by free carriers, resulting in fewer traps. However, if the slope of the ideality factor is less than 1, it is not dependent on light intensity, and trap states are passivated. The ideality factor without an HTL is 1.58 kT/q, indicating a relatively high presence of traps, which adversely affects FF and $V_{OC}$. In contrast, Mg:PSS and Pd:PSS show values of 1.01 kT/q and 0.54 kT/q, respectively, which are close to or less than 1. This suggests that there are few traps, potentially benefiting the device. However, the low $V_{OC}$ and an ideality factor less than 1 kT/q indicate that the results are not dependent on light intensity, making the ideality factor values unreliable [40]. Nevertheless, the ideality factors of Mg:PSS and Pd:PSS blended with PEDOT are 1.36 kT/q and 1.39 kT/q, respectively, closer to 1, indicating bimolecular recombination with fewer traps, resulting in higher $V_{OC}$ and FF.

To understand the impact of Mg:PSS and Pd:PSS on the hole transport mechanism of solar cells, we measured the hole injection barrier (HIB) using UPS. Fig. 3 show the UPS spectra measured by stacking the active layer (PTB7), at various thicknesses on the hole transport layers (HTLs) of Mg:PSS, Pd:PSS, and PEDOT:PSS blends. Detailed XPS and UPS spectra, along with data on the thickness of the PTB7 film, are provided in the Supporting Information (Figs. S3–S5). Changes in the hole injection barrier at the HTL/PTB7 interface provide strong evidence for the extent of p-type doping and the direction of band bending in the active layer. We found that the changes in HIB at the Mg:PSS/PTB7 and Pd:PSS/PTB7 interfaces were very small, at 0.03 eV and 0.05 eV, respectively. This indicates minimal band bending and a low degree of p-type doping at the interface with the active layer. As a result, electrons are not completely blocked and can still diffuse back toward the HTL. This increases the likelihood of carrier recombination, which can negatively impact device parameters and aligns with the low efficiency observed in devices using single Mg:PSS and Pd:PSS. Changes in the HIB of PTB7 with varying thicknesses on blended Mg:PSS and Pd:PSS were also observed. As the thickness of the PTB7 film on the blended Mg:PSS and Pd:PSS substrates increased, the highest occupied molecular orbital (HOMO) level relative to the Fermi level increased by 0.27 eV and 0.18 eV, respectively. This indicates significant band bending and a substantial degree of p-type doping when PEDOT:PSS is blended. As a result, the hole extraction barrier is reduced, creating an ohmic contact with the active layer and suppressing recombination. This allows efficient hole extraction at the interface of Mg:PEDOT:PSS, Pd:PEDOT:PSS, and PTB7, suppressing electron back-diffusion and increasing the overall efficiency of the device.

Detailed data on the HIB with varying thicknesses of PTB7 are clearly shown in Fig. 4. Specific data for the HOMO and lowest occupied molecular orbital (LUMO) levels relative to the Fermi level are presented in Fig. 4(a). The bandgap of PTB7 used for barrier calculation was determined to be 2.25 eV based on combined measurements from inverse photoemission spectroscopy (IPES) and UPS [42]. Mg:PSS has a similar HIB, ranging from 0.718 eV at thin thicknesses to 0.73 eV at thicker thicknesses. Pd:PSS shows a slightly better p-doping ability in the active layer with HIB ranging from 0.616 eV (thin) to 0.728 eV (thick) compared to Mg:PSS, but the differences in device parameters are minimal due to the similar HIB values. Both Mg:PSS and Pd:PSS exhibit very weak band bending, resulting in a straight line with no curvature (Fig. 4b). This indicates that the flat band seen in Mg:PSS and Pd:PSS adversely affects device parameters due to carrier recombination. Strong band bending at the HTL/active layer interface occurs

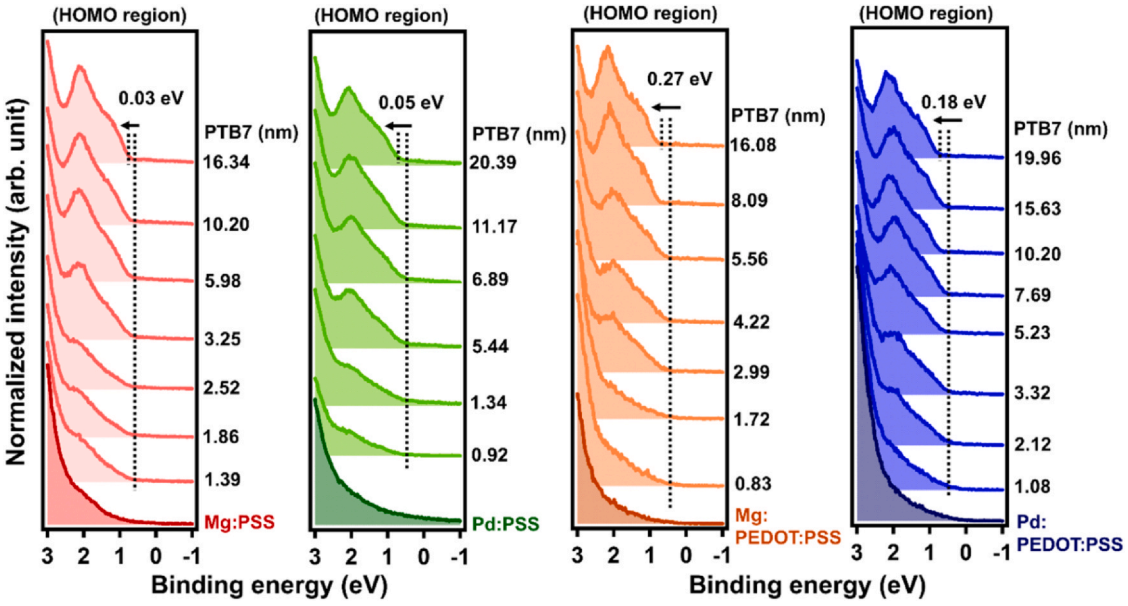


**Fig. 3.** UPS HOMO region of PTB7 with varying thicknesses on substrates of Mg:PSS, Pd:PSS, and PEDOT:PSS blends. PEDOT:PSS = poly (3,4-ethylenedioxythiophene): poly (styrene sulfonate); UPS = ultraviolet photoelectron spectroscopy.

when PEDOT:PSS is mixed with the HTL. The HIB of the PTB7 layer on the Mg:PEDOT:PSS substrate increases from 0.471 eV to 0.641 eV as the thickness increases. A similar trend is observed for the PTB7 layer on the Pd:PEDOT:PSS substrate, with the HIB increasing from 0.40 to 0.613 eV. This demonstrates stronger band bending and p-doping with the addition of PEDOT:PSS, thereby enhancing hole extraction toward the substrate. The band structure and strong hole extraction ability are much more favorable for hole extraction (Fig. 4c). Consequently, when PEDOT:PSS blended Mg:PSS and Pd:PSS are positioned between the HTL and PTB7, they block electrons and reduce interfacial recombination.

## 4. Summary

In conclusion, we investigated the application of novel HTLs integrating Mg and Pd metals with the organic polymer PSS in OSCs. When used alone, these HTLs exhibited various drawbacks; however, by blending with the benchmark material PEDOT:PSS, these shortcomings could be mitigated, leading to improved efficiency. UPS and XPS measurements provided a detailed understanding of the interfacial energy level alignment, electronic band structure, and band bending at the HTL/PTB7 interface. These HTLs, when used independently, displayed limitations with efficiencies of 6.232% and 5.836% for Mg:PSS and Pd:PSS, respectively. The low $V_{OC}$ and FF were attributed to Auger recombination under light intensity, and UPS and XPS also indicated that the hole extraction capability of PTB7 was hindered, leading to recombination at the barrier. However, blending these HTLs with PEDOT:PSS mitigated these issues and significantly improved device performance, achieving efficiencies of 8.356% and 8.303% for Mg:PEDOT:PSS and Pd:PEDOT:PSS, respectively. This improvement resulted from enhanced hole extraction capability through the formation of an ohmic contact at the HTL/PTB7 interface and reduced current

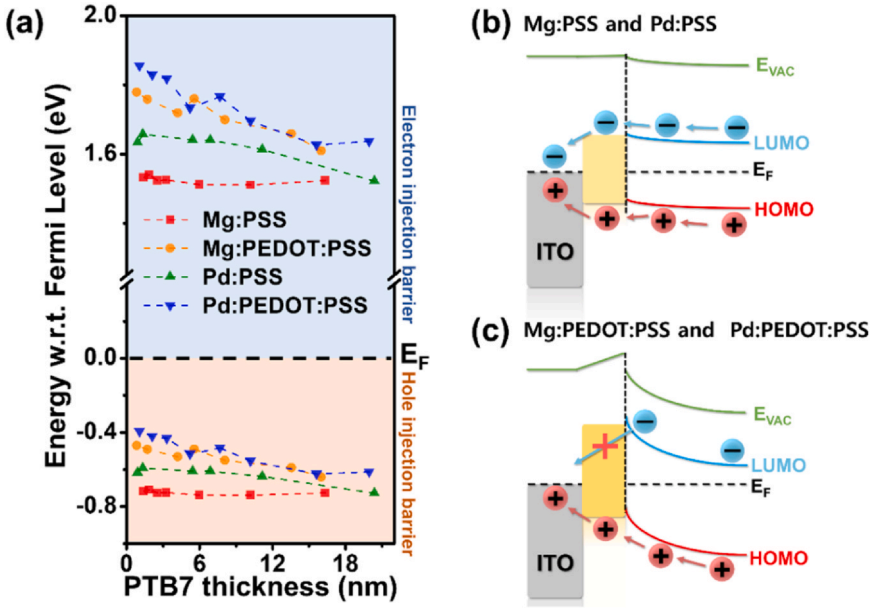


**Fig. 4.** (a) Energy level diagram and p-doping effect with varying thicknesses of PTB7, (b) Schematic of the electronic structure of Mg:PSS and Pd:PSS, (c) Schematic of the electronic structure with PEDOT:PSS blending. PEDOT:PSS = poly (3,4-ethylenedioxythiophene): poly (styrene sulfonate).

leakage due to higher shunt resistance and lower series resistance, as observed in dark current measurements. This study demonstrates that the mixed structures of organic materials and metals in the interfacial layers of organic solar cells can influence the energy band structure depending on the metal used. This insight aids in designing better HTLs by selecting various metals or organic materials for improved performance.

## Declaration of Competing Interest

The authors declare that they have no known competing financial interests or personal relationships that could have appeared to influence the work reported in this paper.

## Acknowledgments

This work was supported by the Basic Study and Interdisciplinary R &D Foundation Fund of the University of Seoul (2023) for Jung Hwa Seo. Also, this work was supported by the 2023 Research Fund of the National Science Foundation (NSF) for Harrison Smith.

## Appendix A. Supporting material

Supplementary data associated with this article can be found in the online version at doi:10.1016/j.nxener.2025.100248.

## References

[1] P. Cheng, X. Zhan, Stability of organic solar cells: challenges and strategies, Chem. Soc. Rev. 45 (2016) 2544–2582, https://doi.org/10.1039/c5cs00593k.
[2] M. Kaltenbrunner, M.S. White, E.D. Głowacki, T. Sekitani, T. Someya, N.S. Sariciftci, S. Bauer, Ultrathin and lightweight organic solar cells with high flexibility, Nat. Commun. 3 (2012) 770, https://doi.org/10.1038/ncomms1772.
[3] M.A. Alkhalayfeh, A.A. Aziz, M.Z. Pakhuruddin, An overview of enhanced polymer solar cells with embedded plasmonic nanoparticles, Renew. Sustain. Energy Rev. 141 (2021) 110726, https://doi.org/10.1016/j.rser.2021.110726.
[4] Y. Miyake, A. Saeki, Machine learning-assisted development of organic solar cell materials: issues, analyses, and outlooks, J. Phys. Chem. Lett. 12 (2021) 12391–12401, https://doi.org/10.1021/acs.jpclett.1c03526.
[5] W. Gao, F. Qi, Z. Peng, F.R. Lin, K. Jiang, C. Zhong, W. Kaminsky, Z. Guan, C.S. Lee, T.J. Marks, H. Ade, A.K.Y. Jen, Achieving 19% power conversion efficiency in planar-mixed heterojunction organic solar cells using a pseudosymmetric electron acceptor, Adv. Mater. 34 (2022) 1–11, https://doi.org/10.1002/adma.202202089.
[6] Y. Wei, Z. Chen, G. Lu, N. Yu, C. Li, J. Gao, X. Gu, X. Hao, G. Lu, Z. Tang, J. Zhang, Z. Wei, X. Zhang, H. Huang, Binary organic solar cells breaking 19% via manipulating the vertical component distribution, Adv. Mater. 34 (2022) 1–8, https://doi.org/10.1002/adma.202204718.
[7] W. Zhu, A.P. Spencer, S. Mukherjee, J.M. Alzola, V.K. Sangwan, S.H. Amsterdam, S.M. Swick, L.O. Jones, M.C. Heiber, A.A. Herzing, G. Li, C.L. Stern, D.M. DeLongchamp, K.L. Kohlstedt, M.C. Hersam, G.C. Schatz, M.R. Wasielewski, L.X. Chen, A. Facchetti, T.J. Marks, Crystallography, morphology, electronic structure, and transport in non-fullerene/non-indacenodithienothiophene polymer: Y6 solar cells, J. Am. Chem. Soc. 142 (2020) 14532–14547, https://doi.org/10.1021/jacs.0c05560.
[8] M. Zhang, X. Guo, W. Ma, H. Ade, J. Hou, A large-bandgap conjugated polymer for versatile photovoltaic applications with high performance, Adv. Mater. 27 (2015) 4655–4660, https://doi.org/10.1002/adma.201502110.
[9] J. Yuan, Y. Zhang, L. Zhou, G. Zhang, H.L. Yip, T.K. Lau, X. Lu, C. Zhu, H. Peng, P.A. Johnson, M. Leclerc, Y. Cao, J. Ulanski, Y. Li, Y. Zou, Single-junction organic solar cell with over 15% efficiency using fused-ring acceptor with electron-deficient core, Joule 3 (2019) 1140–1151, https://doi.org/10.1016/j.joule.2019.01.004.
[10] Y. Meng, Z. Hu, N. Ai, Z. Jiang, J. Wang, J. Peng, Y. Cao, Improving the stability of bulk heterojunction solar cells by incorporating pH-neutral PEDOT:PSS as the hole transport layer, ACS Appl. Mater. Interfaces 6 (2014) 5122–5129, https://doi.org/10.1021/am500336s.
[11] J. Cameron, P.J. Skabara, The damaging effects of the acidity in PEDOT:PSS on semiconductor device performance and solutions based on non-acidic alternatives, Mater. Horiz. 7 (2020) 1759–1772, https://doi.org/10.1039/c9mh01978b.
[12] J. Lee, H. Kang, S. Kee, S.H. Lee, S.Y. Jeong, G. Kim, J. Kim, S. Hong, H. Back, K. Lee, Long-term stable recombination layer for tandem polymer solar cells using self-doped conducting polymers, ACS Appl. Mater. Interfaces 8 (2016) 6144–6151, https://doi.org/10.1021/acsami.5b11742.
[13] J.J. Lee, S.H. Lee, F.S. Kim, H.H. Choi, J.H. Kim, Simultaneous enhancement of the efficiency and stability of organic solar cells using PEDOT:PSS grafted with a PEGME buffer layer, Org. Electron. 26 (2015) 191–199, https://doi.org/10.1016/j.orgel.2015.07.022.
[14] K.H. Girish, K.A. Vishnumurthy, T.S. Roopa, Role of conducting polymers in enhancing the stability and performance of perovskite solar cells: a brief review, Mater. Today Sustain. 17 (2022) 100090, https://doi.org/10.1016/j.mtsust.2021.100090.
[15] S. Tajik, H. Beitollahi, F.G. Nejad, I.S. Shoaie, M.A. Khalilzadeh, M.S. Asl, Q. Van Le, K. Zhang, H.W. Jang, M. Shokouhimehr, Recent developments in conducting polymers: applications for electrochemistry, RSC Adv. 10 (2020) 37834–37856, https://doi.org/10.1039/d0ra06160c.
[16] B. Walker, H. Choi, J.Y. Kim, Interfacial engineering for highly efficient organic solar cells, Curr. Appl. Phys. 17 (2017) 370–391, https://doi.org/10.1016/j.cap.2016.12.007.
[17] A. Guerrero, S. Chambon, L. Hirsch, G. Garcia-Belmonte, Light-modulated TiOx interlayer dipole and contact activation in organic solar cell cathodes, Adv. Funct. Mater. 24 (2014) 6234–6240, https://doi.org/10.1002/adfm.201401233.
[18] Y. Sun, C.J. Takacs, S.R. Cowan, J.H. Seo, X. Gong, A. Roy, A.J. Heeger, Efficient, air-stable bulk heterojunction polymer solar cells using $MoO_X$ as the anode interfacial layer, Adv. Mater. 23 (2011) 2226–2230, https://doi.org/10.1002/adma.201100038.
[19] C. Zuo, L. Ding, Solution-processed $Cu_2O$ and CuO as hole transport materials for efficient perovskite solar cells, Small 11 (2015) 5528–5532, https://doi.org/10.1002/smll.201501330.
[20] W. Chen, F.Z. Liu, X.Y. Feng, A.B. Djurišić, W.K. Chan, Z.B. He, Cesium doped $NiO_X$ as an efficient hole extraction layer for inverted planar perovskite solar cells, Adv. Energy Mater. 7 (2017) 1–8, https://doi.org/10.1002/aenm.201700722.
[21] J.H. Seo, A. Gutacker, Y. Sun, H. Wu, F. Huang, Y. Cao, U. Scherf, A.J. Heeger, G.C. Bazan, Improved high-efficiency organic solar cells via incorporation of a conjugated polyelectrolyte interlayer, J. Am. Chem. Soc. 133 (2011) 8416–8419, https://doi.org/10.1021/ja2037673.
[22] K. Yuan, L. Chen, Y. Chen, Versatile electron-collecting interfacial layer by in situ growth of silver nanoparticles in nonconjugated polyelectrolyte aqueous solution for polymer solar cells, J. Phys. Chem. B 118 (2014) 11563–11572, https://doi.org/10.1021/jp506869q.
[23] G.E. Lim, Y.E. Ha, M.Y. Jo, J. Park, Y.C. Kang, J.H. Kim, Nonconjugated anionic polyelectrolyte as an interfacial layer for the organic optoelectronic devices, ACS Appl. Mater. Interfaces 5 (2013) 6508–6513, https://doi.org/10.1021/am400478b.
[24] Y. Bai, Q. Dong, Y. Shao, Y. Deng, Q. Wang, L. Shen, D. Wang, W. Wei, J. Huang, Enhancing stability and efficiency of perovskite solar cells with crosslinkable silane-functionalized and doped fullerene, Nat. Commun. 7 (2016) 12806, https://doi.org/10.1038/ncomms12806.
[25] S. Daskeviciute-Geguziene, A. Magomedov, M. Daskeviciene, K. Genevičius, N. Nekrašas, V. Jankauskas, K. Kantminiene, M.D. McGehee, V. Getautis, Cross-linkable carbazole-based hole transporting materials for perovskite solar cells, Chem. Commun. 58 (2022) 7495–7498, https://doi.org/10.1039/d2cc02612k.
[26] Q.D. Yang, J. Li, Y. Cheng, H.W. Li, Z. Guan, B. Yu, S.W. Tsang, Graphene oxide as an efficient hole-transporting material for high-performance perovskite solar cells with enhanced stability, J. Mater. Chem. A Mater. 5 (2017) 9852–9858, https://doi.org/10.1039/c7ta01752a.
[27] H. Shi, C. Liu, Q. Jiang, J. Xu, Effective approaches to improve the electrical conductivity of PEDOT:PSS: a review, Adv. Electron. Mater. 1 (2015) 1–16, https://doi.org/10.1002/aelm.201500017.
[28] G. Greczynski, T. Kugler, M. Keil, W. Osikowicz, M. Fahlman, W.R. Salaneck, Photoelectron spectroscopy of thin films of PEDOT-PSS conjugated polymer blend: a mini-review and some new results, J. Electron Spectros. Relat. Phenom. 121 (2001) 1–17, https://doi.org/10.1016/S0368-2048(01)00323-1.
[29] Z. Fan, J. Ouyang, Thermoelectric properties of PEDOT:PSS, Adv. Electron. Mater. 5 (2019) 1–23, https://doi.org/10.1002/aelm.201800769.
[30] T.R. Lv, W.H. Zhang, Y.Q. Yang, J.C. Zhang, M.J. Yin, Z. Yin, K.T. Yong, Q.F. An, Micro/nano-fabrication of flexible poly(3,4-ethylenedioxythiophene)-based conductive films for high-performance microdevices, Small 19 (2023) 2301071, https://doi.org/10.1002/smll.202301071.
[31] H. Chen, Z. Yin, Y. Ma, D. Cai, Q. Zheng, Solution-processed polymer bilayer heterostructures as hole-transport layers for high-performance opaque and semi-transparent organic solar cells, Mater. Today Energy 35 (2023) 101322, https://doi.org/10.1016/j.mtener.2023.101322.
[32] Z. Wang, R. Liu, PEDOT:PSS-based electrochromic materials for flexible and stretchable devices, Mater. Today Electron. 4 (2023) 100036, https://doi.org/10.1016/j.mtelec.2023.100036.
[33] Q. Li, Y. Sun, C. Yang, K. Liu, M.R. Islam, L. Li, Z. Wang, S. Qu, Optimizing the component ratio of PEDOT:PSS by water rinse for high efficiency organic solar cells over 16.7, Sci. Bull. (Beijing) 65 (2020) 747–752, https://doi.org/10.1016/j.scib.2019.12.021.
[34] F. Shoukat, J.H. Kang, Y. Khan, Y.J. Park, J.H. Lee, B. Walker, J.H. Seo, Solution-processed metal ion polyelectrolytes as hole transport materials for efficient inverted perovskite solar cells, Adv. Mater. Interfaces 10 (2023) 2300043, https://doi.org/10.1002/admi.202300043.
[35] J.H. Lee, Y. Khan, S. Kim, A.J. Choi, B. Walker, S. Park, J.H. Seo, Photoelectron spectroscopic study of the interfacial electronic structures of metal-ion containing polyelectrolytes on ITO substrates, Adv. Funct. Mater. 34 (2024) 2315074, https://doi.org/10.1002/adfm.202315074.
[36] A.K.K. Kyaw, D.H. Wang, V. Gupta, W.L. Leong, L. Ke, G.C. Bazan, A.J. Heeger, Intensity dependence of current-voltage characteristics and recombination in high-efficiency solution-processed small-molecule solar cells, ACS Nano 7 (2013) 4569–4577, https://doi.org/10.1021/nn401267s.
[37] T. Singh, T. Miyasaka, Stabilizing the efficiency beyond 20% with a mixed cation perovskite solar cell fabricated in ambient air under controlled humidity, Adv. Energy Mater. 8 (2018) 1700677, https://doi.org/10.1002/aenm.201700677.
[38] Z. Li, W. Wang, N.C. Greenham, C.R. McNeill, Influence of nanoparticle shape on charge transport and recombination in polymer/nanocrystal solar cells, Phys.

Chem. Chem. Phys. 16 (2014) 25684–25693, https://doi.org/10.1039/c4cp01111b.
[39] G.A.H. Wetzelaer, M. Kuik, M. Lenes, P.W.M. Blom, Origin of the dark-current ideality factor in polymer: fullerene bulk heterojunction solar cells, Appl. Phys. Lett. 99 (2011) 153506, https://doi.org/10.1063/1.3651752.
[40] D. Zhao, M. Sexton, H.Y. Park, G. Baure, J.C. Nino, F. So, High-efficiency solution-processed planar perovskite solar cells with a polymer hole transport layer, Adv. Energy Mater. 5 (2015) 1401855, https://doi.org/10.1002/aenm.201401855.
[41] S. Shao, Z. Chen, H.H. Fang, G.H. Ten Brink, D. Bartesaghi, S. Adjokatse, L.J.A. Koster, B.J. Kooi, A. Facchetti, M.A. Loi, N-type polymers as electron extraction layers in hybrid perovskite solar cells with improved ambient stability, J. Mater. Chem. A Mater. 4 (2016) 2419–2426, https://doi.org/10.1039/c5ta10696f.
[42] S. Park, J. Jeong, G. Hyun, M. Kim, H. Lee, Y. Yi, The origin of high PCE in PTB7 based photovoltaics: proper charge neutrality level and free energy of charge separation at PTB7/$PC_{71}BM$ interface, Sci. Rep. 6 (2016) 35262, https://doi.org/10.1038/srep35262.